Experimental investigation of puffing/microexplosion in fuel droplets and effects of injection modes on it.

Zuhaib Nissar* [1], A Rashid A Aziz[2], Morgan R Heikal[2, 3], Mhadi A Ismael[1]

[1] *Center for Automotive Research and Electric Mobility (CAREM), Universiti Teknologi PETRONAS, 32610 Seri Iskandar, Perak, Malaysia*
[2] *Center for Automotive Research and Electric Mobility (CAREM), Universiti Teknologi PETRONAS, 32610 Seri Iskandar, Perak, Malaysia*
[3] *Sir Harry Ricardo Laboratories, Advanced Engineering Centre, School of Computing, Engineering and Mathematics, University of Brighton, Brighton BN2 4GJ, UK*

*Corresponding author: zuhaib_16000073@utp.edu.my

Abstract. Puffing/microexplosion potentially increases atomization and enables better air-fuel mixing in sprays, thereby improving combustion. In this paper, we have investigated the physics leading to puffing and microexplosion in fuel droplets and identified factors such as droplet detachment modes and droplet-air interaction that influence puffing/microexplosion. A microsyringe is used to inject droplets as small as 100 μm radius in a control volume chamber maintained at 500℃ and atmospheric pressure. Droplet dynamics are captured using high-speed camera coupled with a long-distance microscopic lens using backlight illumination technique as the droplet traverses and undergoes puffing and microexplosion. In-house image processing codes are used to track droplet motion and compute its geometrical parameters, which enable us to decipher microexplosion dynamics. During this study, two significant factors were identified to cause puffing/microexplosion; thinning of droplet shell and interfacial instabilities. A general trend of increasing puffing times was observed with increasing droplet radii. The modes of detachment do affect the instabilities at the droplet surface which further amplify them and causes early puffing. Furthermore, the rate of bubble growth was amplified for the droplets traversing at higher Reynolds number.

1. Introduction

The use of fuels like water in diesel emulsion (WIDE) as a fuel source is attractive due to its ability to reduce NOx and soot particles, its use in combustion engines also obviates the environmental concerns of greenhouse gas emission and carbon sequestration. The addition of water lowers the local flame temperature which reduces NOx emissions [1, 2]. As water evaporates, it supplies hydroxy (OH) radicals to the combustion process thereby reducing soot formation [3]. These emulsions increased brake thermal efficiency by 6%, with a 30% reduction in NOx and particulate emissions, and 70% reduction in unburnt hydrocarbons [4, 5]. It has been found that immiscible emulsions like water in diesel undergo a phenomenon called puffing/microexplosion due to difference in the volatilities of their components. Microexplosions can be beneficial to secondary atomization and enhance penetration depth of fuel sprays in internal combustion engines.

Microexplosion phenomenon is caused due to the effect of diffusional entrapment of volatile component, i.e. water, inside an emulsion droplet [6]. When WIDE droplet is heated under high-temperature conditions, evaporation of diesel at the surface leads to the development of boundary layer.

In contrary to this, droplet core has a higher concentration of water which heats up gradually to surpass its boiling point and become superheated. According to thermodynamics there is a maximum superheat limit a liquid can accumulate called critical limit. This condition is metastable until the superheated water attains the critical limit. At nucleation temperature, the metastable state breaks, and formation of a new vapour phase takes place in the form of small vapour bubbles. If nucleation temperature coincides with the critical limit, it is called homogeneous nucleation. Otherwise, nucleation which occurs before the critical limit is called heterogeneous nucleation [7]. Bubbles which have radius less than that of their critical radii will collapse. These bubbles combine to form a giant bubble. With intense surge in internal pressure, the bubble pinches through the droplet surface, which causes ebullition of an emulsion droplet. If the phenomenon is extensive, it is called microexplosion, while as, if it is limited to a portion of an emulsion droplet, it is called puffing [8, 9]. These minion droplets lead to enhancement in the net surface area which in turn accelerates the gasification process and may help in homogenizing charge in internal combustion engines [10]. Different models have been suggested to estimate the times to puffing, also called microexplosion delay time which is based on the penetration of heat inside the droplet [11]. However, the significant gap between the predicted times to puffing and the experimental values has been left unaddressed.

In the view of above considerations, we have investigated the physics of puffing/microexplosion in WIDE droplets. We have enquired the role of droplet generation modes and interaction between droplet and air on the microexplosion delay time. Details of the experimental setup are described in the next section. The analysis performed on the experimental data is presented in section 3. The results of the experimentally observed puffing/microexplosion in WIDE droplets are discussed in section 4. The results are summarized in section 5.

2. Working Principles

Shadowgraphy mainly deals with the optics of inhomogeneous medium [12]. The inhomogeneities and disturbances may occur due to the motion of bulk matter, turbulence, and thermal convection. These disturbances may lead to small changes in the density gradient and with it the refractive index. Refractive index n is given by

$$n = \frac{c_0}{c} \tag{2.1}$$

where $c_0 = 3 \times 10^8 \ m/s$ is the universal speed limit, c is the speed of light in the medium.
A well-known Gladstone–Dale relation is used to link the density of fluid ρ and its refractive index.

$$\frac{n-1}{\rho} = k, \tag{2.2}$$

where k is the Gladstone-Dale coefficient.
If a geometrical light ray traverses in the z-direction, the optical inhomogeneities refract or bend light rays in proportion to the gradients of refractive index in an *x-y* plane (wave-front) [12]. The resulting ray curvature is given by

$$\frac{\partial^2 x}{\partial z^2} = \frac{1}{n}\frac{\partial n}{\partial x} \qquad ; \qquad \frac{\partial^2 y}{\partial z^2} = \frac{1}{n}\frac{\partial n}{\partial y} \tag{2.3}$$

Integrating along the optical axis z, components of the angular ray deflection in the x and y directions can be written as:

$$\varepsilon_x = \frac{L}{n_0}\frac{\partial n}{\partial x}; \qquad \varepsilon_y = \frac{L}{n_0}\frac{\partial n}{\partial y} \tag{2.4}$$

where L is the optical path length, n_0 is the refractive index of the surrounding medium.
In shadowgraphy, illuminance level in the image responds to the second spatial derivative of refractive index, i.e. $\frac{\partial^2 n}{\partial x^2}$ and $\frac{\partial^2 n}{\partial y^2}$. It displays the ray displacement resulting from the deflection and is thus a mere

shadow. This can be seen in Figure 1. However, it allows us to visualise the most noticeable features of a subject with little changes in illumination.
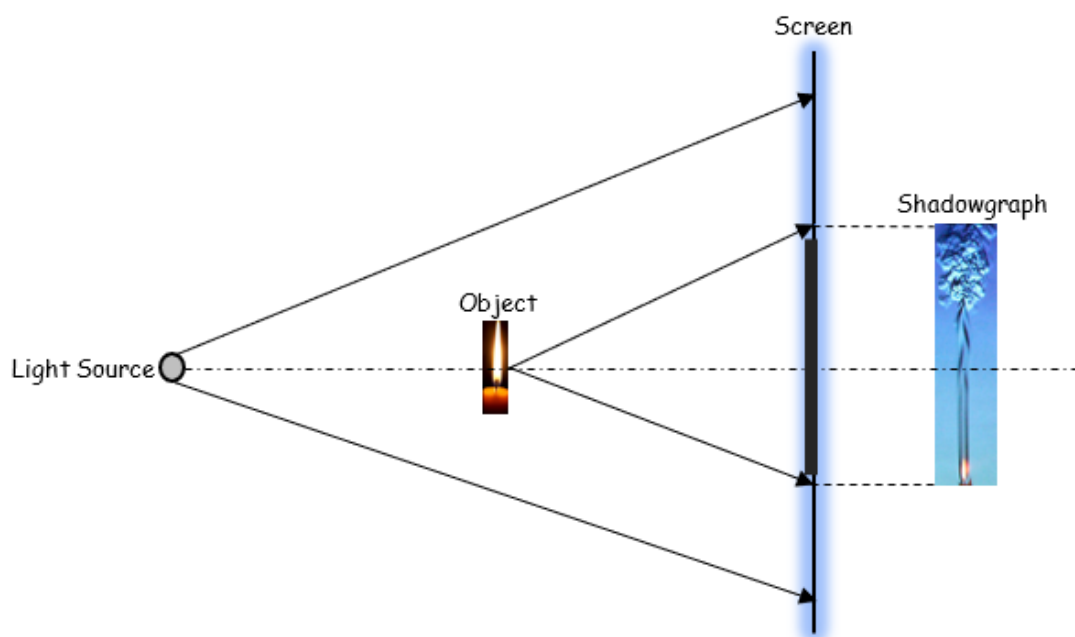

Figure 1. Schematic showing the principles of Shadowgraphy.

3. Experimental Procedure

Experiments are carried out at Flow Visualization Laboratory, Universiti Teknologi PETRONAS, Malaysia. Primary purpose of these experiments is to gather decipher puffing/microexplosion dynamics in order to relate them with different approaches to model the phenomenon. The setup consists of a constant volume combustion chamber, which is maintained at a constant ambient temperature of 500 °C and atmospheric pressure. The schematic of the experimental setup is given in Figure 2. The cylindrical chamber has an opening for fuel injection and is mounted with a ceramic electric heater. The heater is connected to a PID controller wired with K-type thermocouple in order to measure and ascertain a specific steady-state gas temperature at the centre of the chamber. The heater is insulated with fibreglass wool to prevent heat losses and the chamber is assembled with borosilicate windows using flanges in order to provide optical access for the flow visualisation.

A lipophilic surfactant (Span 80 – 1% volume of water) is used as an emulsifier to prepare 15% (v/v) water in diesel emulsion. The mixture is mechanically stirred for 10 min at 1000 rpm to homogenise the emulsion. The experiment involves injection of free-falling emulsion droplets using a micro-pump UMP3 with Micro4 Controller. This controller would allow us to monitor injection time and amount of fuel and subsequently produce droplets of regular size. The needle is positioned at the inlet once the steady-state temperature is achieved inside the chamber. This is done to prevent any heat transfer at the needle-tip before injection.

The optical setup consisted of a Multi LED (LT-V8-15) (Tokyo, Japan) for back illumination, high-speed video camera (Phantom Miro M310) (Wayne, NJ, USA) coupled with a long-distance microscope (Infinity K2) (Boulder, CO, USA) and zoom lens (CF1 objective) (Boulder, CO, USA). The camera is adjusted to a resolution of 256×800 pixel², the frame rate of 12,000 fps and exposure time of 2 µs. The image scale factor is calculated using the measurements from the diameter of the syringe needle, which is known to us as 0.3 mm. The uncertainties in the microexplosion delay time are associated with the least count of the optical setup (1/12000 s). The uncertainty for the measurement of the droplet diameter is related to the detection of the droplet perimeter, which is estimated to be ±37 µm. Droplets with
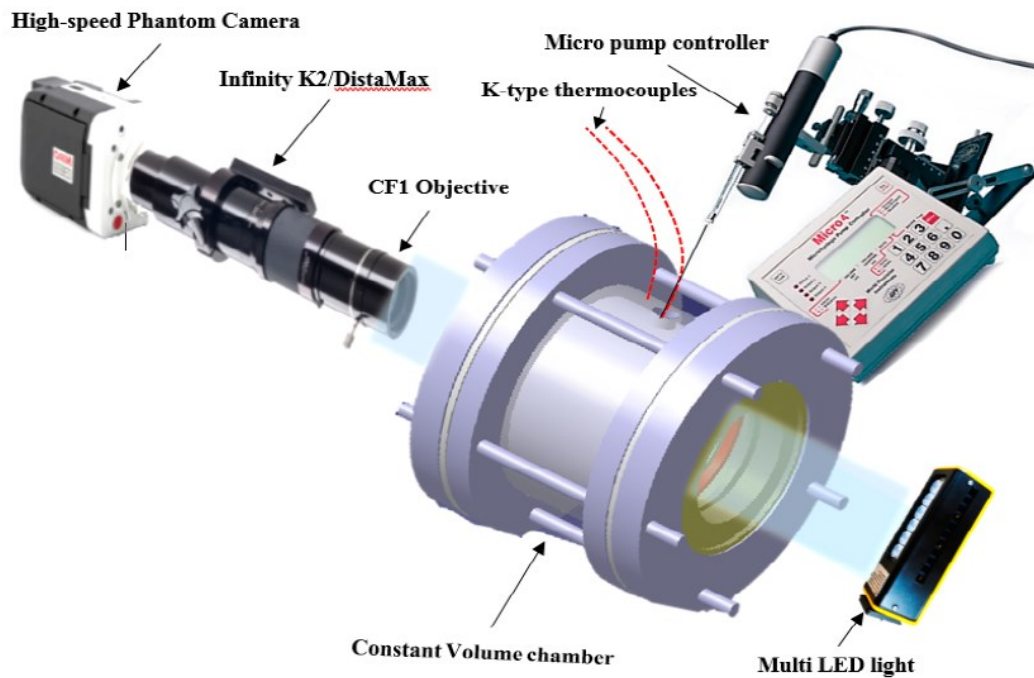
Figure 2. Schematic of the combustion chamber showing the optical accesses and the long-distance microscope imaging system. The Multi LED light used to provide the back illumination. Reprinted from Energies, Volume 11, No. 9, Ismael et al., Investigation of Puffing and Micro-Explosion of Water-in-Diesel Emulsion Spray Using Shadow Imaging, P 2281, Copyright MDPI (2018).

diameters smaller than 50 μm are ignored due to the large experimental uncertainty. The uncertainty in velocity measurements is estimated based on the reports and assessments published earlier, according to which the global uncertainty is less than 2% even under supersonic applications [13].

4. Analysis

In this study, different sets of time-lapse images are prepared for different droplet diameters, starting from the droplet injection point until the aftermaths of microexplosion. Using in-house codes for digital image processing, motion and trajectory of the droplets are tracked and their geometrical parameters are evaluated simultaneously. The stack of images are imported to a Java-based image processing program called ImageJ for pre-processing [14]. Pre-processing consists of a series of matrix operations, namely, image contrast enhancement, filter operations, thresholding, morphology operations, feature detection, and segmentation. ImageJ considers each image as a graphics object where each element of the matrix contains three colour intensities, red, green, and blue (RGB) values. The RGB images are processed to 8-bit greyscale images in which each pixel is represented with numerical value from a list of $2^8 = 256$ values. This value is assigned by linearly scaling from min-max to 0-255, such that 0 and 255 usually represent white and black spots, respectively.

For detecting edges, the Sobel filter is used to highlight sharp changes in the intensity of the image. In this, two 3×3 convolution kernels (as shown below) are used to generate vertical and horizontal derivatives. The final image is produced by combining the two derivatives using the square root of the sum of the squares [15, 16].

$$\begin{bmatrix} 1 & 2 & 1 \\ 0 & 0 & 0 \\ -1 & -2 & -1 \end{bmatrix} \qquad \begin{bmatrix} 1 & 0 & -1 \\ 2 & 0 & -2 \\ 1 & 0 & -1 \end{bmatrix}$$

This is followed by a thresholding operation. Thresholding is a type of image segmentation that isolates objects by converting a grey-scale image into a binary image. In this operation, the two levels are assigned to pixels that are below or above the specified threshold value. Pixels with luminance greater than this specified threshold value are assigned value 1 (white) and value 0 (black) if otherwise.
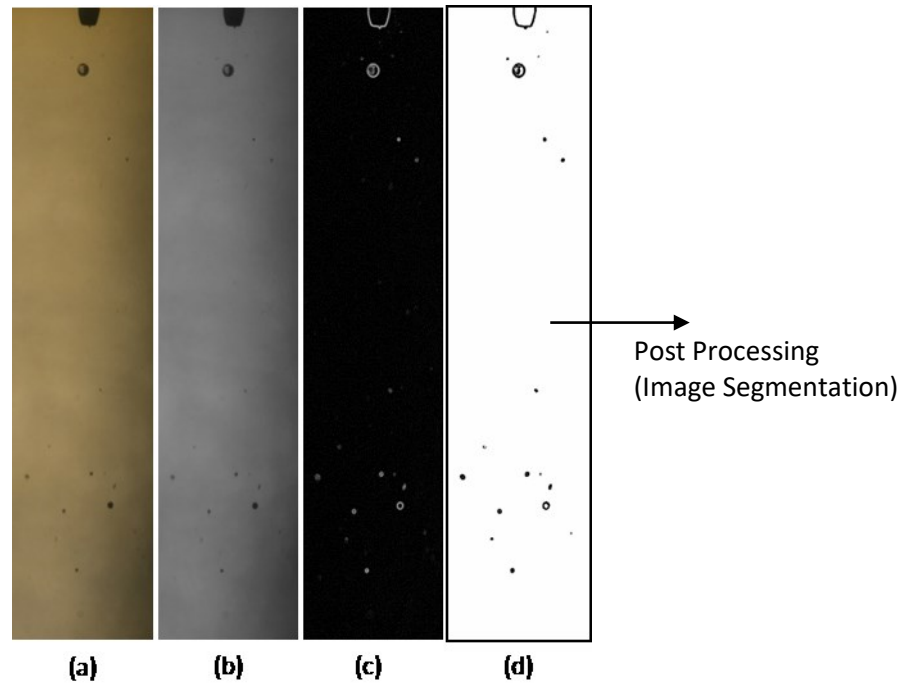
Figure 3. Chronology of image processing operations, where (a) Original image, (b) 8-bit Grayscale image, (c) Sobel filter for edge detection, (d)Binary image using threshold feature

Figure 3 demonstrates the order of the aforementioned operations performed for the time-lapsed images of emulsion droplets.

During post-processing, the periphery of the droplet is captured from the binary image and tracked for the entire stack of images using in-house codes. This allows us to measure different geometrical parameters of the droplet such as area, radius, droplet centroid, perimeter, shape factor and aspect ratio, thereby enabling us to ascertain droplet dynamics.

5. Results and discussion

In this section, results of investigation during droplet detachment and after it are presented and dynamics of droplets leading to microexplosion/puffing are explained based on the evolution of droplet parameters such as radius, motion, geometry and shape factor. The significant results are provided and discussed as follows:

5.1. Effects of Droplet Detachment

It is observed that microexplosion is sensitively dependent on the modes through which these droplets are detached which is also supportive to the experiments by Wang et al. [2]. As the droplet is detached from the syringe tip, its mode of generation and preliminary deformation induce instabilities at the surface. This appears to effect microexplosion delay time as will be seen later. Two modes of detachment are identified during experiments, stable and unstable. Stable mode is characterized by uniform striations or vertical ribs along the droplet crown exhibiting symmetry and reduced shape deformations at the surface after detachment, while in unstable mode there are either irregular striations or no striations at all along the crown, the contours are very asymmetric and deformations are intense after the detachment. During detachment these rib-like structures undergo buckling leading to atomization, thus forming child droplets and a bigger droplet near the syringe tip.

Stable 1   **Stable 2**   **Unstable 1**   **Unstable 2**

Time (s)

1/12000 s

(a)   (b)   (c)   (d)
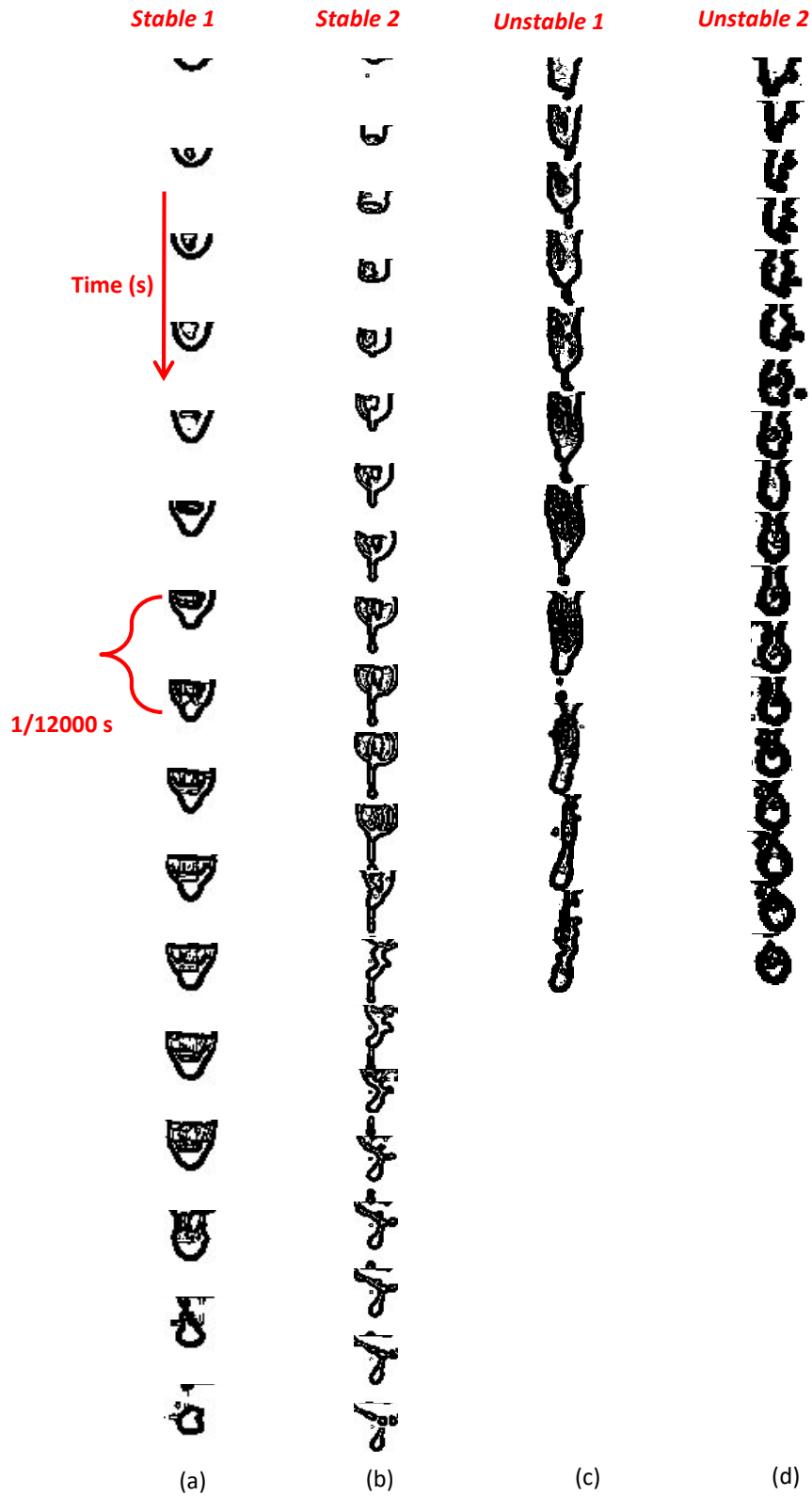
Figure 4. Image sequences showing different droplet detachment modes at ambient temperature of 500 °C and 101.325 kPa. Time interval between frames is 1/12000 s; (a) and (b) refer to stable modes, (c) and (d) refer to unstable modes

5.2. Droplet Dynamics

As the droplet undergoes free fall, heat from the ambient air penetrates inside the droplet causing internal nucleation. During the experiments, it is observed that internal nucleation occurred faster during unstable droplet detachment mode. It is hard to assume homogeneous nucleation as there are many factors contributing to the formation of bubble nucleus inside the droplet much of which are probabilistic in nature. This also includes cavitation due to in-syringe flow effects. Oza and Sinnamon [17, 18] called it an internal mode of nucleation. There were test runs in which the nucleation seems to have occurred prior to droplet detachment which is also confirmed in the literature. Analysis of these effects requires investigation of in-syringe flow effects.

Figure 7 shows the genesis and growth of droplet due to nucleation and bubble expansion. A bubble nucleus forms at 17/6000 s which expands due to bubble pressure leading to thinning of liquid shell around the droplet, and at 62/6000 s the droplet undergoes puffing giving away child droplets. It is observed that a single bubble nucleus forms close to the droplet centre in most cases, however, droplets containing binary bubble nuclei are observed as well (see Figure 5). These observations are consistent with the experiments by Wang et al. [2].


**Figure 5.** Image showing two bubble nuclei being formed inside the droplet

Using in-house codes for image processing, motion and dynamics of the droplets is traced. Figure 6(a) shows the trajectory of droplets right from the tip of the syringe till the point where they undergo puffing. In order to estimate the average velocity of droplets, displacement of the droplet centroid is plotted against time. In Figure 6(b) velocities of these droplets range from 0.1 m/s to 1.7 m/s. Based on the values of initial droplet diameter $2R_{d0}$ and their velocity V, droplet Reynolds number $Re = \frac{2\rho_{air} \cdot V \cdot R_{d0}}{\mu_{air}}$ is calculated. Properties of air are evaluated for $T_g = 500°C$; dynamic viscosity of air $\mu_{air} = 35.47 \times 10^{-6}$ Pa/s and its density $\rho_{air} = 0.4567$ kg/m^3.

(a)

(b)
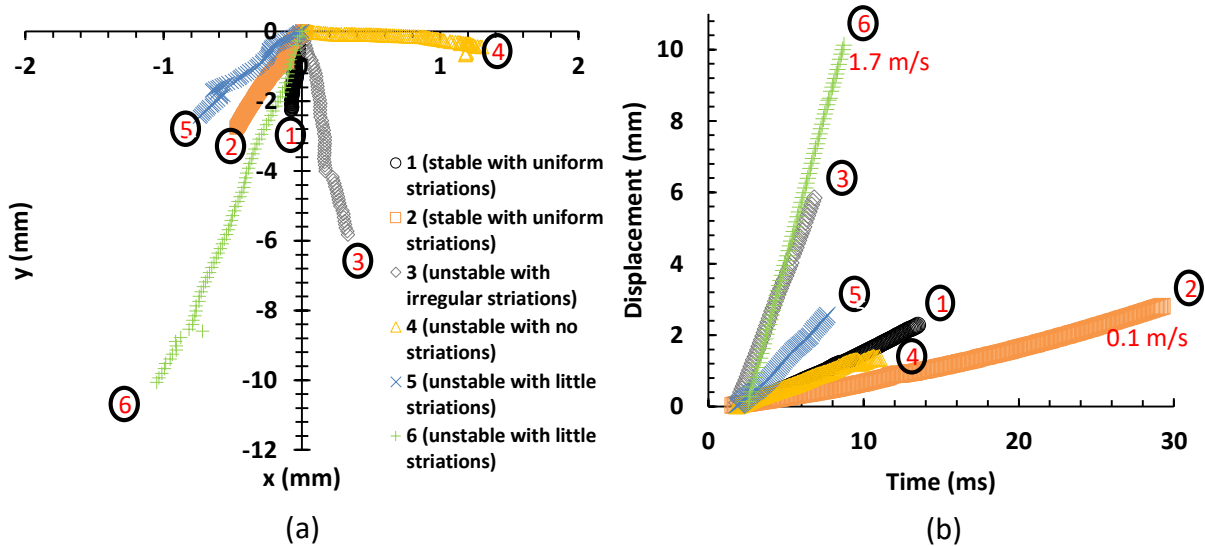
Figure 6. (a) Trajectories of droplets during free fall inside the constant volume chamber at $500°C$ and 101.325 kPa; (b) Plots describing the motion of droplets
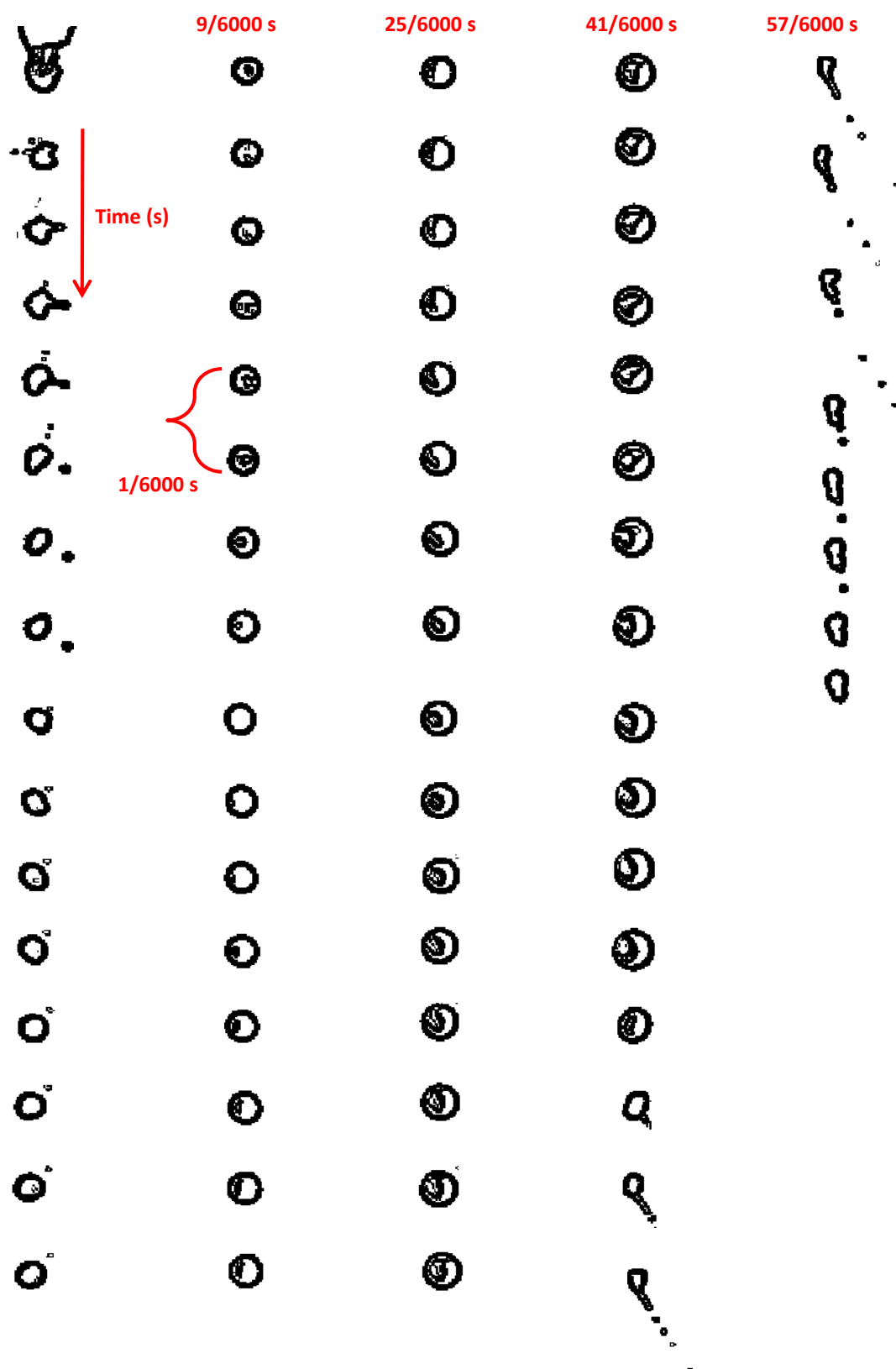
Figure 7. Image sequence showing droplet of $2R_{d0} = 200$ μm undergoing bubble expansion and puffing. Time interval between frames is 1/6000 s.
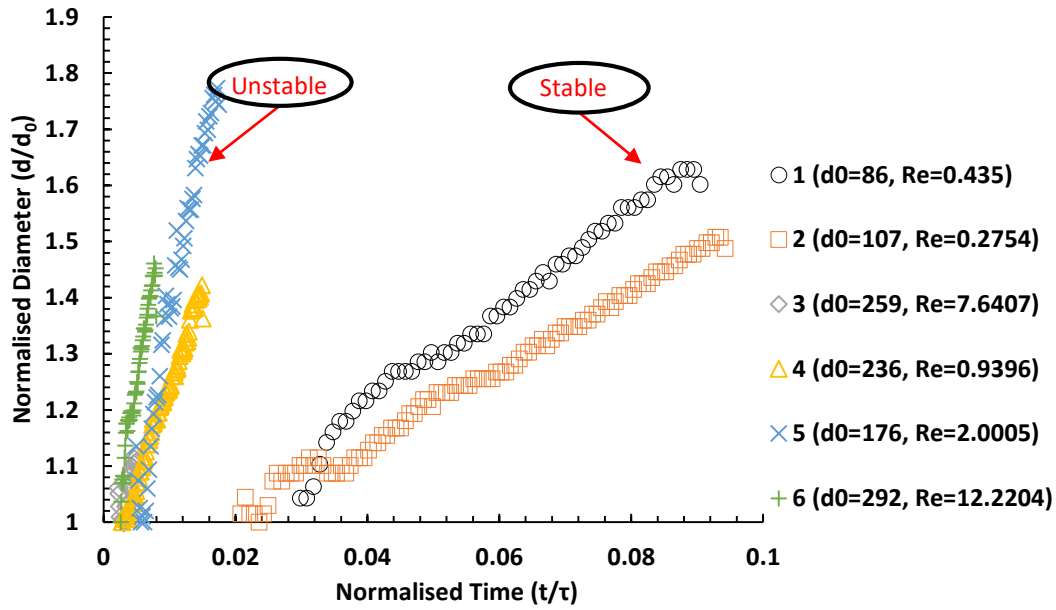
Figure 8. History of droplets undergoing bubble expansion. Normalized diameter vs normalized time, where $\tau = R_0^2/\kappa$. Details of droplet detachment mode, initial diameter d_0 (μm) and Reynolds number Re are given on the right.

Figure 8 shows variations of droplet diameter with time, which gives us insights towards puffing regardless of droplet diameter. Time is normalised with the thermal diffusion time scale (τ) of the emulsion droplet, where $\tau = R_0^2/\kappa$, $\kappa = 8.7335 \times 10^{-8}$ m^2/s is the thermal diffusivity of the emulsion mixture whose value is evaluated for initial droplet temperature $T_0 = 40\ °C$. One can see that bubble expansion inside the droplet causes an increase in the droplet diameter thereby causing thinning of the droplet shell and eventually leading to puffing/microexplosion. It is observed that the timescale of puffing is much less than the diffusion timescale. Two regimes of droplet expansion are recognized which are mainly related to the modes of droplet detachment and also the magnitude of droplet Reynolds number. In case of unstable detachment, puffing is found to occur quite earlier while as in stable mode the same effect is prolonged. Also, while comparing curves 1 and 2, it is observed that droplets falling at higher Reynolds numbers appear to have higher rates of droplet expansion. Similar trend could be seen for the unstable regime. This can be partly attributed to increasing rates of heat transfer due to convection and internal circulation at higher Reynolds numbers.

To investigate further on these modes, evolution of shape factors of the droplets with time were examined. The results are presented in Figure 9, where (1), (2) are observed as stable modes while the rest refer to unstable modes of generation. It can be seen from these figures that there are very little fluctuations in the amplitude in case of stable mode causing longer times to puffing. In unstable mode, these fluctuations appear to be intense causing shorter times to puffing. Also, it is observed that droplet takes longer to detach from the syringe tip in case of stable mode.

It is deciphered that the modes of droplet detachment and motion of the droplet induce instabilities at the droplet surface which give rise to droplet oscillations and undulations thereby causing wrinkling at the droplet surface. This allows the bubble to reach the droplet surface due to intense bubble pressure and cause thinning of the liquid shell at the surface, finally punching through it much earlier than anticipated. This is consistent with the results in [19] in which experimental values of times to puffing were always shorter than the predicted values. Based on this, two factors were identified to cause puffing/microexplosion; thinning of the liquid shell and interfacial instabilities. The modes of detachment and Reynolds number affect these instabilities which can further amplify them and cause early puffing. Furthermore, the rate of bubble growth is amplified for the droplets traversing at higher Reynolds numbers.
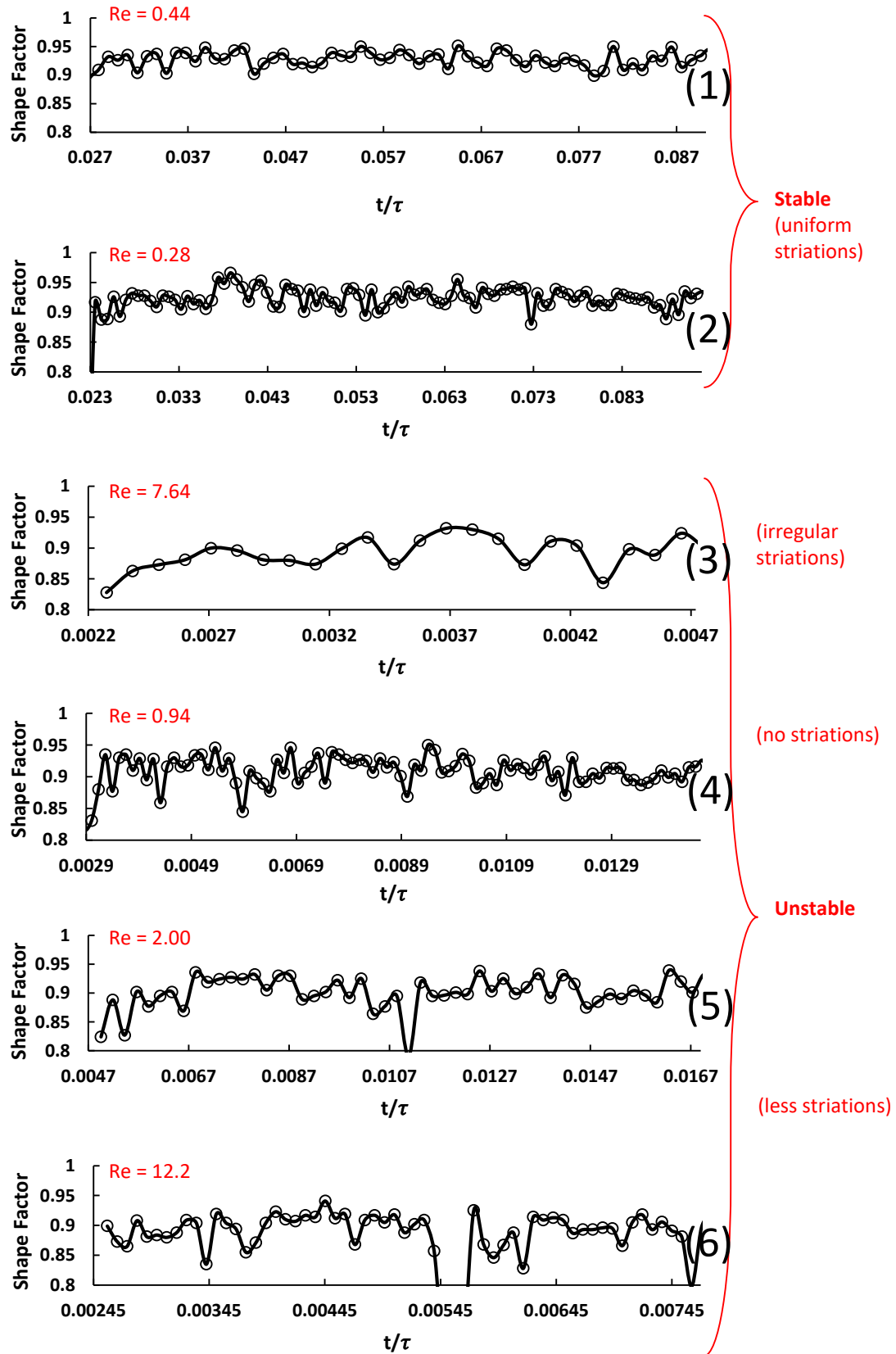
Figure 9. Fluctuations in the shape factor of the droplet with time; (1)-(6) are in the same order as in the previous figure.

6. Conclusion

Droplets of water in diesel emulsion were visualised using backlight illumination technique as they traversed hot ambient. The events of puffing/microexplosion were captured at 12000 fps with the help of high-speed camera which was coupled with a microscopic lens. Using in house codes for image processing, dynamics of the droplets were traced, and their geometrical parameters were evaluated. Bubble nucleation was observed shortly after the bubble had detached from the microsyringe. As the bubble increased in size, it caused swelling of the droplet and eventually led to puffing. Thinning of the liquid shell and droplet oscillations were found to be the primary cause which led to puffing/microexplosion. A general trend of increasing puffing times with increasing droplet diameters was observed, although in all cases. Two regimes of droplet puffing were observed as the normalised values of droplet diameter and time were compared. The modes of detachment were found to affect the instabilities at droplet surfaces which can lead to early puffing. Furthermore, the rate of bubble growth was amplified for the droplets at higher Reynolds numbers.

References

[1]   C. K. Law, C. H. Lee, and N. Srinivasan, "Combustion characteristics of water-in-oil emulsion droplets," *Combustion and Flame,* vol. 37, pp. 125-143, 1980, doi: https://doi.org/10.1016/0010-2180(80)90080-2.

[2]   C. H. Wang, X. Q. Liu, and C. K. Law, "Combustion and microexplosion of freely falling multicomponent droplets," *Combustion and Flame,* vol. 56, no. 2, pp. 175-197, 1984, doi: https://doi.org/10.1016/0010-2180(84)90036-1.

[3]   I. Glassman, R. A. Yetter, and N. G. Glumac, *Combustion*. Academic Press, 2015.

[4]   O. A. Elsanusi, M. M. Roy, and M. S. Sidhu, "Experimental Investigation on a Diesel Engine Fueled by Diesel-Biodiesel Blends and their Emulsions at Various Engine Operating Conditions," *Applied Energy,* vol. 203, pp. 582-593, 2017, doi: https://doi.org/10.1016/j.apenergy.2017.06.052.

[5]   A. M. A. Attia and A. R. Kulchitskiy, "Influence of the structure of water-in-fuel emulsion on diesel engine performance," *Fuel,* vol. 116, pp. 703-708, 2014, doi: https://doi.org/10.1016/j.fuel.2013.08.057.

[6]   A. Miglani, S. Basu, and R. Kumar, "Insight into instabilities in burning droplets," *Physics of Fluids,* vol. 26, no. 3, p. 032101, 2014, doi: https://doi.org/10.1063/1.4866866.

[7]   A. Faghri and Y. Zhang, *Transport Phenomena in Multiphase Systems*. Boston: Academic Press, 2006.

[8]   H. Watanabe and K. Okazaki, "Visualization of secondary atomization in emulsified-fuel spray flow by shadow imaging," *Proceedings of the Combustion Institute,* vol. 34, no. 1, pp. 1651-1658, 2013, doi: https://doi.org/10.1016/j.proci.2012.07.005.

[9]   M. A. Ismael, M. R. Heikal, A. R. A. Aziz, M. El-Adawy, Z. Nissar, M. B. Baharom, E. Z. A. Zainal, Firmansyah, and C. Crua, "Investigation of puffing and micro-explosion of water-in-diesel emulsion spray using shadow imaging," *Energies,* vol. 11, no. 9, p. 2281, 2018, doi: https://doi.org/10.3390/en11092281.

[10]   C. K. Law, *Combustion Physics*. Cambridge: Cambridge University Press, 2006.

[11]   S. S. Sazhin, O. Rybdylova, C. Crua, M. Heikal, M. A. Ismael, Z. Nissar, and A. R. B. A. Aziz, "A simple model for puffing/micro-explosions in water-fuel emulsion droplets," *International Journal of Heat and Mass Transfer,* vol. 131, pp. 815-821, 2019, doi: https://doi.org/10.1016/j.ijheatmasstransfer.2018.11.065.

[12]   G. S. Settles, *Schlieren and Shadowgraph Techniques*. Berlin, Heidelberg: Springer, 2001.

[13] C. Robbe, N. Nsiampa, A. Oukara, and A. Papy, "Quantification of the uncertainties of high-speed camera measurements," *International Journal of Metrology and Quality Engineering,* vol. 5, no. 2, pp. 201(1-9), 2014, doi: https://doi.org/10.1051/ijmqe/2014007.

[14] J. Schindelin, I. Arganda-Carreras, E. Frise, V. Kaynig, M. Longair, T. Pietzsch, S. Preibisch, C. Rueden, S. Saalfeld, B. Schmid, J.-Y. Tinevez, D. J. White, V. Hartenstein, K. Eliceiri, P. Tomancak, and A. Cardona, "Fiji: an open-source platform for biological-image analysis," *Nature Methods,* vol. 9, no. 7, pp. 676-682, 2012, doi: https://doi.org/10.1038/nmeth.2019.

[15] I. Sobel and G. Feldman, "A 3x3 isotropic gradient operator for image processing," in *Pattern Classification and Scene Analysis, R. Duda and P. Hart, Eds.*: John Wiley & Sons, 1973, pp. 271-272.

[16] D. Anoraganingrum, "Cell segmentation with median filter and mathematical morphology operation," 1999: IEEE, doi: https://doi.org/10.1109/iciap.1999.797734.

[17] R. D. Oza and J. F. Sinnamon, "An Experimental and Analytical Study of Flash-Boiling Fuel Injection," 1983: SAE International, doi: https://doi.org/10.4271/830590.

[18] R. D. Oza, "On the Mechanism of Flashing Injection of Initially Subcooled Fuels," *Journal of Fluids Engineering,* vol. 106, no. 1, pp. 105-109, 1984, doi: https://doi.org/10.1115/1.3242383.

[19] Z. Nissar, O. Rybdylova, S. S. Sazhin, M. Heikal, A. R. B. A. Aziz, and M. A. Ismael, "A model for puffing/microexplosions in water/fuel emulsion droplets," *International Journal of Heat and Mass Transfer,* vol. 149, pp. 119-208, 2020, doi: https://doi.org/10.1016/j.ijheatmasstransfer.2019.119208.